

¹ Environmental Science Center, Peking University, Beijing, P.R. of China

² Department of Numerical Forecasting, Japan Meteorological Agency, Otatemachi, Tokyo, Japan

Recycling of suspended particulates by the interaction of sea-land breeze circulation and complex coastal terrain

H. Choi¹, Y. H. Zhang¹, and S. Takahashi²

With 11 Figures

Received April 27, 2003; revised July 11, 2003; accepted August 22, 2003

Published online: June 2, 2004 © Springer-Verlag 2004

Summary

The dispersion of recycled particulates in the complex coastal terrain surrounding Kangnung city, Korea was investigated using a three-dimensional non-hydrostatic numerical model and lagrangian particle model (or random walk model). The results show that particulates at the surface of the city that float to the top of thermal internal boundary layer (TIBL) are then transported along the eastern slope of the mountains with the sea breeze passage and nearly reach the top of the mountains. Those particulates then disperse eastward at this upper level over the coastal sea and finally spread out over the open sea. Total suspended particulate (TSP) concentration near the surface of Kangnung city is very low. At night, synoptic scale westerly winds intensify due to the combined effect of the synoptic scale wind and land breeze descending the eastern slope of the mountains toward the coast and further seaward. This increase in speed causes development of internal gravity waves and a hydraulic jump up to a height of about 1 km above the surface over the city. Particulate matter near the top of the mountains also descends the eastern slope of the mountains during the day, reaching the central city area and merges near the surface inside the nocturnal surface inversion layer (NSIL) with a maximum ground level concentration of TSP occurring at 0300 LST. Some particulates are dispersed following the propagation area of internal gravity waves and others in the NSIL are transported eastward to the coastal sea surface, aided by the land breeze. The following morning, particulates dispersed over the coastal sea from the previous night, tend to return to the coastal city of Kangnung with the sea breeze, developing a recycling process and combine with emitted

surface particulates during the morning. These processes result in much higher TSP concentration. In the late morning, those particulates float to the top of the TIBL by the intrusion of the sea breeze and the ground level TSP concentration in the city subsequently decreases.

1. Introduction

During the past decade empirical and numerical studies have been carried out on the prediction of pollutant concentrations over complex coastal terrain, but their accuracy in relation to the dispersion and diffusion of particulate matter contains uncertainties, due to complicated wind patterns caused by topography and the ocean (Choi, 2003; Diehl et al, 1982; Kimura and Yoshikawa, 1988). Suspended particulates are not only harmful to human health but are also of great importance in the heat budget of the coastal atmospheric boundary layer. A high density of suspended particulates near the top of the convective boundary layer reduces the solar energy reaching the surface and the reduction of solar radiation, such as the dome effect.

Kuwagata and Sumioka (1991) explained that a local circulation system was very complicated due to the interaction of complex terrain and the

adjacent sea under differing weather conditions. Ross et al (1999) indicated that the local air shed surrounding the Comalco smelter was strongly influenced by the proximity of the ocean and the complex terrain of the Tama Valley. An increase in pollution concentration occurred from daytime processes involving photochemical reactions in the city (Baird, 1995) and pollutant gases could be changed into the aerosol phase by their chemical reaction processes and cause an increase in local and regional air pollution concentrations (Moller, 2001). Park and Moon (2001) explained particle dispersion in the complex coastal terrain of Korea by using a lagrangian particle model. Xuan (1999) describes how a high density of suspended particulates interrupts daytime convective processes near the surface and causes a decrease in vertical mixing in the boundary layer and a subsequent increase in total suspended particulate concentration.

The computation of dust emission factors representative of the city area is very difficult due to the problem of lack of necessary input data such as emission rate, chemical processes among different species, and meteorological impact on the transportation and diffusion of particulates (PU, 1995). Therefore, this study was mainly confined to investigating how total suspended particulate concentration could vary as a consequence of the recycling process in the complex coastal terrain of southern Korea, using a three-dimensional meteorological model and random walk model.

2. Numerical analysis and data

A three-dimensional non-hydrostatic grid point model in a terrain following coordinate system (x, y, z^*) , called the LASV-5 model, originally developed at the Japan Meteorological Institute (Takahashi, 1995), was adopted for a 48 hour numerical simulation on meteorological phenomena from 0900 LST, August 13 to 0900 LST, August 15, 1995 on a Hitachi super computer. Two domains were used, consisting of 50×50 grid points with a uniform horizontal interval for the course mesh (20 km) and also 50×50 grid points for the fine mesh (5 km) with one-way double nesting. There were 16 levels in the vertical spread from 10 m to 6 km with sequentially larger intervals between levels with

increasing altitude. Twelve hourly global analysis data of wind, potential temperature, specific humidity and atmospheric pressure analyzed by JMA were horizontally and vertically interpolated onto the two coarse and fine mesh grids. Initial sea surface temperature data for the model were provided from satellite-derived analyses (NFRADA, 1998).

2.1 Meteorological model

LASV-5, which was originally developed at the Meteorological Research Institute, Japan Meteorological Agency, consists of a three-dimensional hydrostatic and non-hydrostatic option with a terrain-following coordinate system (x, y, z^*) based upon the Boussinesq and anelastic approximations (Kimura and Arakawa, 1983; Kimura and Takahashi, 1991). The equations of motion can be derived as

$$\frac{dhu}{dt} = fhv - h\Theta \frac{\partial \pi'}{\partial x} + \Theta(z_T - z^*) \frac{\partial z_G}{\partial x} \frac{\partial \pi'}{\partial z^*} + \frac{z_T^2}{h} \frac{\partial}{\partial z^*} \left(K_m \frac{\partial u}{\partial z^*} \right), \quad (1)$$

$$\frac{dhv}{dt} = -fhu - h\Theta \frac{\partial \pi'}{\partial x} + \Theta(z_T - z^*) \frac{\partial z_G}{\partial y} \frac{\partial \pi'}{\partial z^*} + \frac{z_T^2}{h} \frac{\partial}{\partial z^*} \left(K_m \frac{\partial v}{\partial z^*} \right), \quad (2)$$

$$\frac{dhw}{dt} = -z_T \Theta \frac{\partial \pi'}{\partial z^*} + gh \frac{\theta'}{\Theta}, \quad (3)$$

$$\frac{d}{dt} = \frac{\partial}{\partial t} + u \frac{\partial}{\partial x} + v \frac{\partial}{\partial y} + w^* \frac{\partial}{\partial z^*},$$

where z^* is the terrain-following vertical coordinate defined as

$$h = z_T - z_G,$$

$$z^* = \frac{z_T(z - z_G)}{h},$$

$$hw^* = z_T w + (z^* - z_T) \left(\frac{\partial z_G u}{\partial x} + \frac{\partial z_G v}{\partial y} \right),$$

$$\theta = T \left(\frac{P_{00}}{P} \right)^{Rd/Cp},$$

$$\theta' = \theta - \Theta,$$

$$\pi = T \left(\frac{P_{00}}{P} \right)^{R_d/C_p},$$

$$\pi' = \pi - \pi,$$

and θ , Θ , T , P_{00} , $-\pi$, π , π' , z , z_T , z_G and K_m are, potential temperature (K), mean potential temperature of the model domain, air temperature at a given height, atmospheric pressure at reference level (=1000 mb), Exner function of the model atmosphere, Exner function of isentropic atmosphere ($\theta = \Theta$), deviation of π , height of upper boundary with its change in time and place in the model domain, height of topography and vertical diffusion coefficient for turbulent momentum ($m^2 s^{-1}$), respectively. The symbols f , g , u , v , w and w^* represent Coriolis parameter, gravity ($m s^{-2}$), velocity components in the x -, y -, z - and z^* -coordinate system, respectively. P , P_{00} , R_d and C_p refer to atmospheric pressure, atmospheric pressure at reference level, gas constant for dry air and specific heat at constant pressure, respectively.

Radiative heating of air from the thermodynamic equation and conservation of water vapor yields

$$\frac{dh\theta'}{dt} = \frac{z_T^2}{h} \frac{\partial}{\partial z^*} \left(K_h \frac{\partial \theta'}{\partial z^*} \right) + hQ_r, \quad (4)$$

$$\frac{dhq}{dt} = \frac{z_T^2}{h} \frac{\partial}{\partial z^*} \left(K_h \frac{\partial q}{\partial z^*} \right). \quad (5)$$

Here, Q_r , θ' and q are radiative heating rate of the atmosphere, potential temperature and specific humidity of water vapor. The continuity equation is

$$\frac{\partial hu}{\partial x} + \frac{\partial hv}{\partial y} + \frac{\partial hw^*}{\partial z^*} = 0. \quad (6)$$

Assuming that the horizontal scale of the phenomena is one of magnitude greater than the vertical scale, Eq. (3) for the hydrostatic equilibrium case can be converted into the following pressure equations as

$$\frac{\partial \pi'}{\partial z^*} = \left(\frac{h}{z_T} \right) \left(\frac{g}{T^2} \right) \theta'. \quad (7)$$

Hydrostatic pressure deviation, π'_H in a non-hydrostatic calculation is

$$\frac{\partial \pi'_H}{\partial z^*} = \left(\frac{h}{z_T} \right) \left(\frac{g}{\Theta^2} \right) \theta', \quad (8)$$

and non-hydrostatic pressure in the non-hydrostatic calculation is given by

$$\begin{aligned} \pi'_N &= \pi' - \pi'_H, \\ \frac{\partial^2 \pi'_N}{\partial x^2} + \frac{\partial^2 \pi'_N}{\partial y^2} + \left\{ \left(\frac{z_T}{z_T - z_G} \right)^2 \right. \\ &+ \left. \left(\frac{z^* - z_T}{h} \right)^2 \left(\left(\frac{\partial z_G}{\partial x} \right)^2 + \left(\frac{\partial z_G}{\partial y} \right)^2 \right) \right\} \\ &\frac{\partial}{\partial z^*} \left(\frac{\partial \pi'_N}{\partial z^*} \right) \\ &+ 2 \left(\frac{z^* - z_T}{h} \right) \frac{\partial z_G}{\partial x} \frac{\partial}{\partial x} \left(\frac{\partial \pi'_N}{\partial z^*} \right) \\ &+ 2 \left(\frac{z^* - z_T}{h} \right) \frac{\partial z_G}{\partial y} \frac{\partial}{\partial y} \left(\frac{\partial \pi'_N}{\partial z^*} \right) \\ &+ \left\{ \left(\frac{z^* - z_T}{h} \right) \left(\frac{\partial}{\partial x} \left(\frac{\partial z_G}{\partial x} \right) + \frac{\partial}{\partial y} \left(\frac{\partial z_G}{\partial y} \right) \right) \right. \\ &+ \left. 2 \left(\frac{z^* - z_T}{h^2} \right) \left(\left(\frac{\partial z_G}{\partial x} \right)^2 + \left(\frac{\partial z_G}{\partial y} \right)^2 \right) \right\} \\ &\frac{\partial}{\partial z^*} \left(\frac{\partial \pi'_N}{\partial z^*} \right) \\ &= \frac{r(x, y, z^*)}{\Theta h}, \end{aligned} \quad (9)$$

where r is expressed by

$$\begin{aligned} r(x, y, z^*) &= \frac{\partial ADVX}{\partial x} + \frac{\partial ADVY}{\partial y} + \frac{z_T}{h} \frac{\partial ADVZ}{\partial z^*} \\ &+ \frac{1}{h} \frac{\partial z_G}{\partial x} \frac{\partial (z^* - z_T) ADVX}{\partial z^*} \\ &+ \frac{1}{h} \frac{\partial z_G}{\partial y} \frac{\partial (z^* - z_T) ADVY}{\partial z^*}, \end{aligned}$$

and

$$\begin{aligned} ADVX &= -\frac{\partial hu u}{\partial x} - \frac{\partial hu v}{\partial y} - \frac{\partial hu w^*}{\partial z^*} + fhv \\ &- \Theta h \frac{\partial \pi'_N}{\partial x} - \Theta (z^* - z_T) \frac{\partial z_G}{\partial x} \left(\frac{\partial \pi'_N}{\partial z^*} \right) \\ &+ \frac{z_T^2}{h} \frac{\partial}{\partial z^*} \left(K_m \frac{\partial u}{\partial z^*} \right), \end{aligned}$$

$$\begin{aligned}
\text{ADVY} &= -\frac{\partial h_{uv}}{\partial x} - \frac{\partial h_{uv}}{\partial y} - \frac{\partial h_{vw}^*}{\partial z^*} - f_{hu} \\
&\quad - \Theta h \frac{\partial \pi'_N}{\partial y} - \Theta (z^* - z_T) \frac{\partial z_G}{\partial y} \left(\frac{\partial \pi'_N}{\partial z^*} \right) \\
&\quad + \frac{z_T^2}{h} \frac{\partial}{\partial z^*} \left(K_m \frac{\partial v}{\partial z^*} \right), \\
\text{ADVZ} &= -\frac{\partial h_{uw}}{\partial x} - \frac{\partial h_{vw}}{\partial y} - \frac{\partial h_{ww}^*}{\partial z^*}.
\end{aligned}$$

The solutions of Eqs. (1), (2), (4), and (5) for the time integration and the vertical direction in the z^* -coordinate were calculated by adopting the Euler-backward scheme and the Crank-Nicholson scheme. The atmospheric pressure changes at the top of a model atmosphere with a material surface were controlled by the wave radiation condition suggested by Klemp and Durran (1983), in order to avoid reflections of gravity waves generated in the lower layers. The periodic lateral boundary condition developed by Orlandi (1976) was applied to the calculation of u , v , θ and q in the model domain. In the numerical simulation, the time interval was set to $\Delta t = 30$ s in the coarse-mesh domain and $\Delta t = 10$ s in the fine-mesh domain, which effectively reduces external gravity waves that appear in the equations, especially for the non-hydrostatic model.

The vertical diffusion coefficients, K_m and K_h for momentum and heat transfer in the surface boundary layer were evaluated from the turbulent closure level-2 model (Yamada, 1983; Yamada and Mellor, 1983). For evaluating total net flux of long wave radiation absorbed by water vapor and carbon dioxide and vertical flux from the surface the H_2O and CO_2 transmission functions, effective vapor amount, specific humidity ($g\text{ cm}^{-2}$), and pressure (mb) at the surface and at several higher levels were considered. Total net solar radiation at the ground as a function of solar zenith angle, latitude, declination and time angle are calculated by the simplified scheme of Katayama (1972) for computing radiative transfer in the troposphere.

Newtonian cooling due to long wave radiation and radiative heating rate for air and soil temperatures near the surface were considered in detail. For the energy budget near the surface, the surface boundary layer was assumed to be a constant flux layer for estimating sensible and

latent heat fluxes and similarity theory was adopted (Businger, 1973; Monin, 1970). On the time variation of soil temperature and specific humidity at the surface, a force restore method suggested by Deardorff (1978) was employed.

2.2 Random walk model

The random walk model (Diehl et al, 1982; Kimura and Yoshikawa, 1988; JMRI, 1995) can be expressed as

$$\begin{aligned}
\Delta x &= u \Delta t, \\
\Delta y &= v \Delta t, \\
\Delta z &= w \Delta t
\end{aligned} \tag{10}$$

and, using coordinates (ξ, η, ζ) , the advection terms can be expressed as

$$\begin{aligned}
u^* &= \frac{\partial \xi}{\partial x} u + \frac{\partial \eta}{\partial x} v + \frac{\partial \zeta}{\partial x} w, \\
v^* &= \frac{\partial \xi}{\partial y} u + \frac{\partial \eta}{\partial y} v + \frac{\partial \zeta}{\partial y} w, \\
w^* &= \frac{\partial \xi}{\partial z} u + \frac{\partial \eta}{\partial z} v + \frac{\partial \zeta}{\partial z} w.
\end{aligned} \tag{11}$$

For the conservation of mass during the advection of particulate matter, it is necessary to transform the three-dimensional wind field calculated from z^* -coordinate system of the LASV-5 model into $z(=z - z_G)$ coordinate system of the random walk model as follows:

$$\begin{aligned}
w^* &= \frac{z^* - h}{h - z_G} \left(\frac{\partial z_G u}{\partial x} + \frac{\partial z_G v}{\partial y} \right) + \frac{h}{h - z_G} w, \\
w^+ &= -\frac{\partial z_G u}{\partial x} - \frac{\partial z_G v}{\partial y} + w.
\end{aligned} \tag{12}$$

The increase in dispersion distribution by diffusion processes of particles with the occurrence probability of each particle as Fickian diffusion is given by

$$d\sigma^2/dt = 2k, \tag{13}$$

and the occurrence probability of particles in uniform random numbers with the same dispersion implies

$$\Delta x = (24k\Delta t)^{1/2} \cdot \text{RND}, \tag{14}$$

where Δx and Δz are similar to Δx and RND is a uniform number in the interval $(-0.5, +0.5)$. If a particle undergoes a random walk with a small

Δt , the particle distribution is assumed to be Gaussian. In the z^* -coordinate system

$$\Delta z^* = (24k\Delta t)^{1/2} \frac{h}{h - z_G} \cdot \text{RND}. \quad (15)$$

For the treatment of deposition processes below the reference level ($z = \Delta z$), the deposition probability of a particle at the ground level can be given as

$$P = \frac{\Delta M}{M} = \frac{v_d \Delta t}{\Delta z}, \quad (16)$$

where v_d is the deposition particle velocity of 0.002 m s^{-1} (Zhang et al, 2001). When no deposition of a particle occurs, a reflection condition is given.

The fine-mesh domain for the particle model consists of 50×50 grid points with a uniform horizontal interval of 5 km, which is the same interval as in the meteorological model. Particles in the model were emitted at the surface in Kangnung city at the rate of four particles per two minutes. After sunset, the number of released particles was reduced to two particles per two minutes, due to the reduced number of

vehicles on the street. Numerically calculated results on suspended particulate concentration were compared with measured TSP-concentrations at Kangnung National University (KNU, 1995).

3. Results and discussion

3.1 Dispersion of suspended particulate (day)

At 1200 LST, 14 August, the prevailing synoptic-scale westerly wind is directed over Mt. Taeguallung toward the coastal sea and the easterly sea-breeze as an upslope or valley wind ascends as far as the top of the mountains. The opposing wind regimes meet along the eastern slope of the mountains. The easterly wind reaches a height of 1400 m before being finally joining up with the westerly as a return flow toward the East Sea (Figs. 1 and 2). The convective boundary layer (CBL) is developed to a thickness of about 1 km above the surface on the upwind side of the mountains, while the thickness of the thermal internal boundary layer (TIBL) is confined to less than 100 m along the eastern slope of the

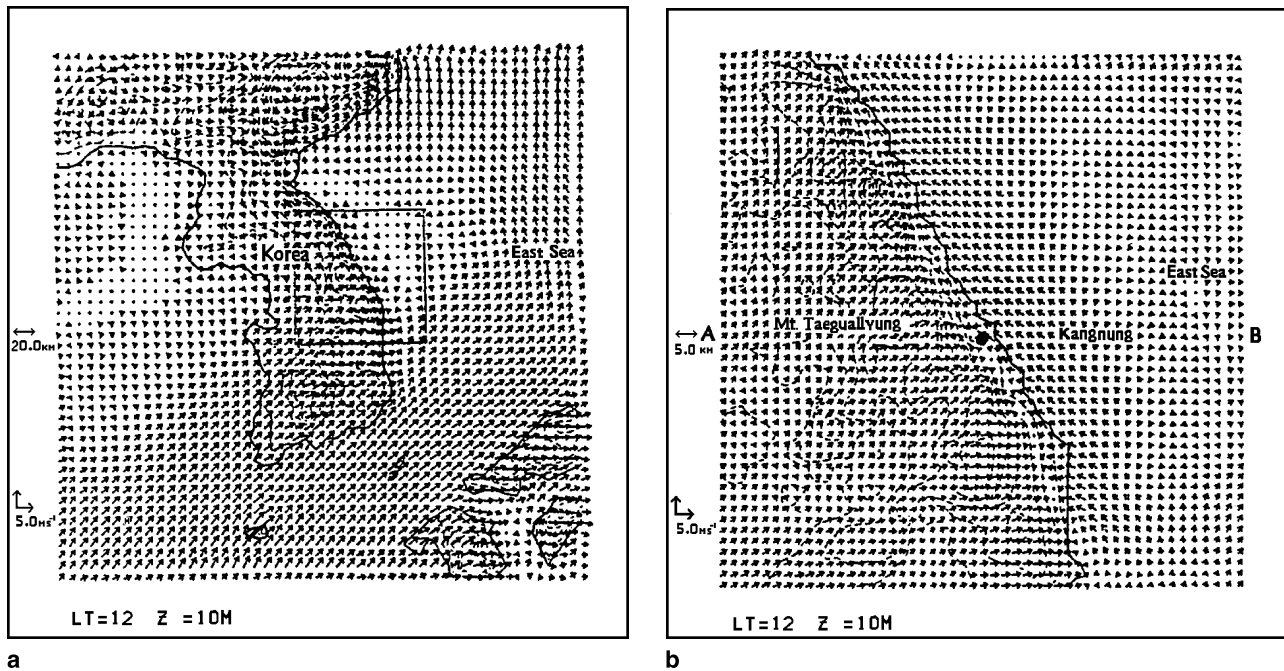


Fig. 1a. Wind speed (m s^{-1}) in the coarse-mesh domain adjacent to the Korean peninsula at 1200 LST, August 14. The thin line (dashed) and circle (open) denote topography and Kangnung city, respectively, **(b)** The fine-mesh domain (5 km), which is indicated in **(a)** by the inset and showing Kangnung city, and, as in **(a)**, consists of 50×50 grid points

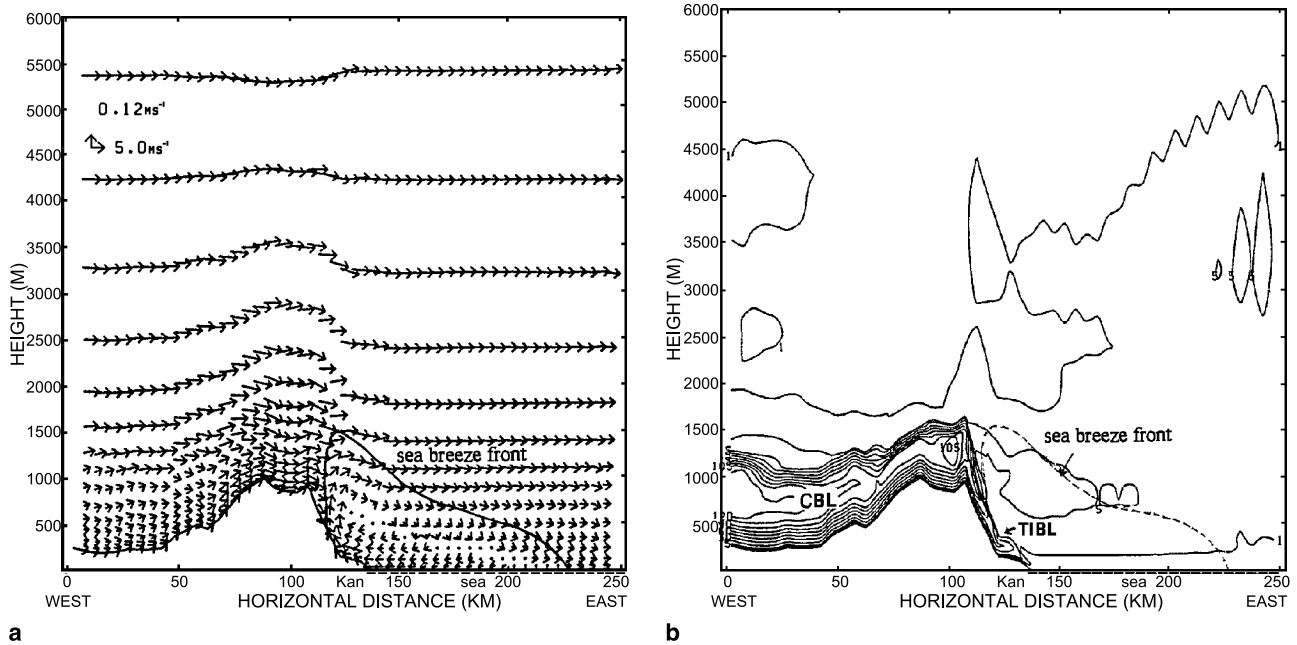


Fig. 2a. Vertical wind profile (m s^{-1}) at 1200 LST, 13 August, 1995 through a line A–B (Mt. Taeguallyung–Kangnung city–East Sea) as indicated in Fig. 1b. Dashed line and Kan denote sea-breeze front and Kangnung city, respectively; **b** Vertical diffusion coefficient for turbulent heat ($\text{m}^2 \text{s}^{-1}$). CBL and TIBL denote convective boundary layer and thermal internal boundary layer. The dashed line on the bottom axis (---) indicates the East Sea

mountains below an easterly sea-breeze circulation, owing to differences in surface roughness and thermal heating at the land-sea interface. At 1500 LST, the atmospheric circulation and the thermal and convective boundary layers are similar in structure to those at 1200 LST.

Also, at this time, suspended particulate matter is transported vertically from the surface of Kangnung city by thermal convection, and then toward the top of the mountains in the uplift provided by the easterly sea breeze. As daytime progresses, the floating particulates, reaching as high as 1400 m, are dispersed eastward below the height of the sea-breeze circulation and then, spread out widely over the coastal sea surface (Fig. 3a). At 1500 LST, the suspended particulates are further dispersed over the coastal sea (Fig. 3b).

3.2 Dispersion of suspended particulates (sunset and night)

At sunset (approximately at 1800 LST), the TIBL becomes thinner owing to the decrease in solar radiation and sea-breeze circulation subsequently becoming weaker than at 1200 LST. The

height of suspended particulates is much lower than at 1500 LST- and TSP-concentration inside the thinner TIBL near Kangnung city becomes higher. Shortly after sunset (at 2100 LST), as internal gravity waves begin to develop along the eastern slope of the mountains, a relatively strong downslope wind (katabatic or mountain wind) blows toward the city, but the sea-breeze circulation still exists on the lee side (Fig. 4). Thus, the particulates descend along the eastern slope of the mountains toward the coast and the concentration of particulates in Kangnung city becomes higher than at 1800 LST (Fig. 5).

At 1700 LST, just before sunset, the CBL has shrunk to a depth of 300 m due to the decrease in solar radiation and is much shallower than that at 1200 LST, thereby allowing the TSP concentration inside the thinner CBL to become higher. Vehicle numbers on the roads increased greatly at the end of the working day and a large amount of gases and particulates were emitted, so the TSP concentration became very high (Figs. 10 and 11). After sunset (1800 LST), the number of vehicles gradually decreased and the particulate emissions also decreased, hence lowering the TSP-concentration.

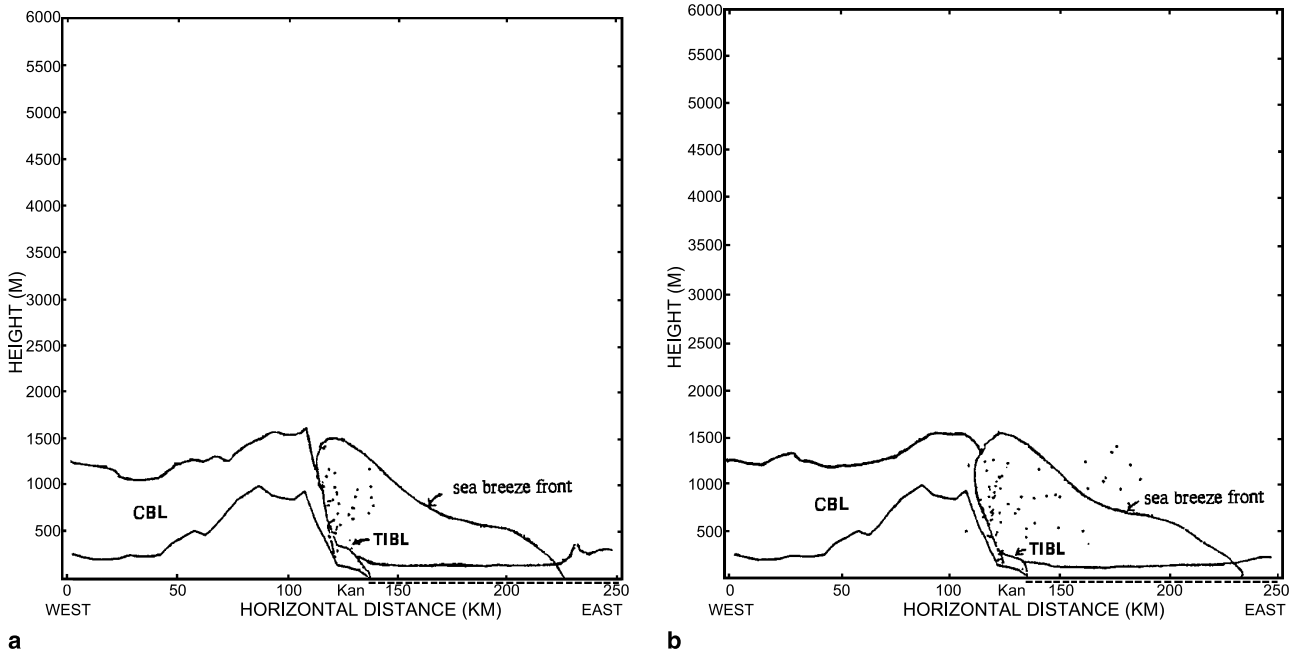


Fig. 3a. Transportation of suspended particulates in the coastal region near Kangnung city (Kan) under the influence of thermal internal boundary layer (TIBL) and upslope wind combined with sea-valley breeze at 1200 LST on August 13, 1995, and **(b)** as in **(a)** except at 1500 LST. CBL denotes convective boundary layer

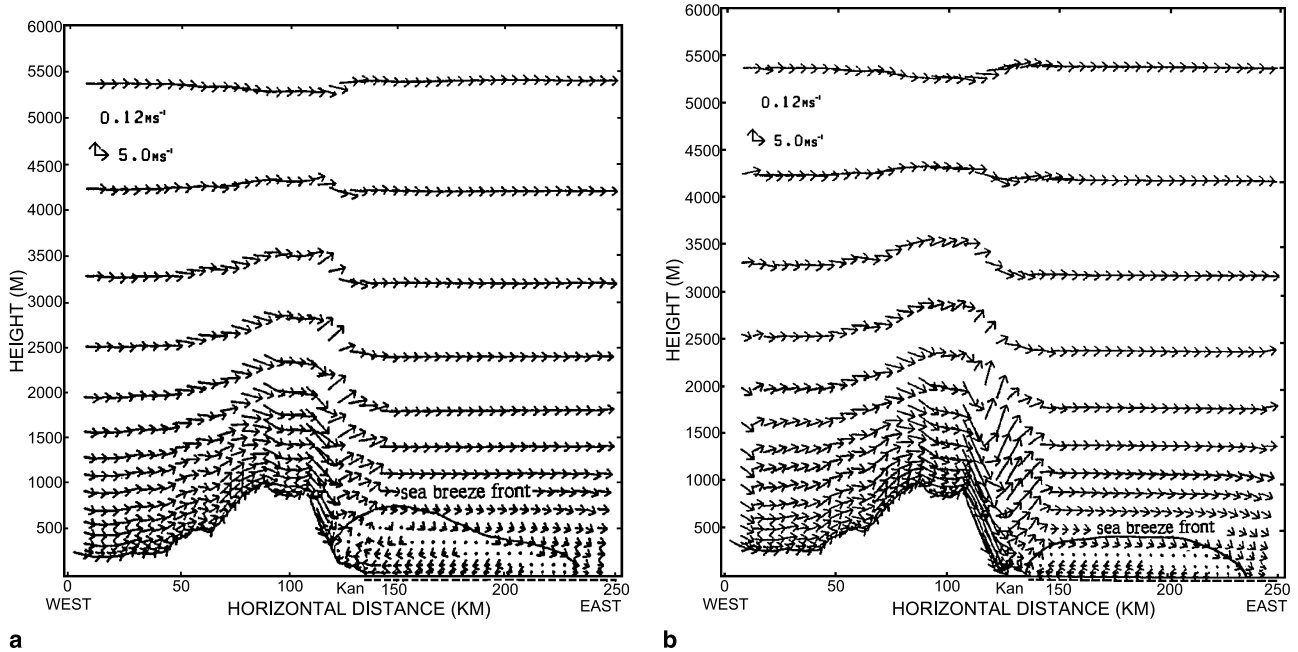


Fig. 4a. Vertical wind profile ($m s^{-1}$) on the line A-B (Mt. Taegualluyng-Kangnung city-East Sea) as indicated in Fig. 2b, showing the influence of the sea breeze circulation at 1800 LST on 14 August, 1995, and **(b)** as in **(a)** except at 2100 LST

On the other hand, at 0000 LST, nocturnal radiative cooling of the surface produces a shallow nocturnal surface inversion layer (NSIL) with a thickness of about 200 m over the coastal

basin, but a relatively thinner thickness of 100 m near the mountains (Figs. 6, 7 and 8). Prevailing westerly downslope winds combined with the westerly land breeze directed toward the sea,

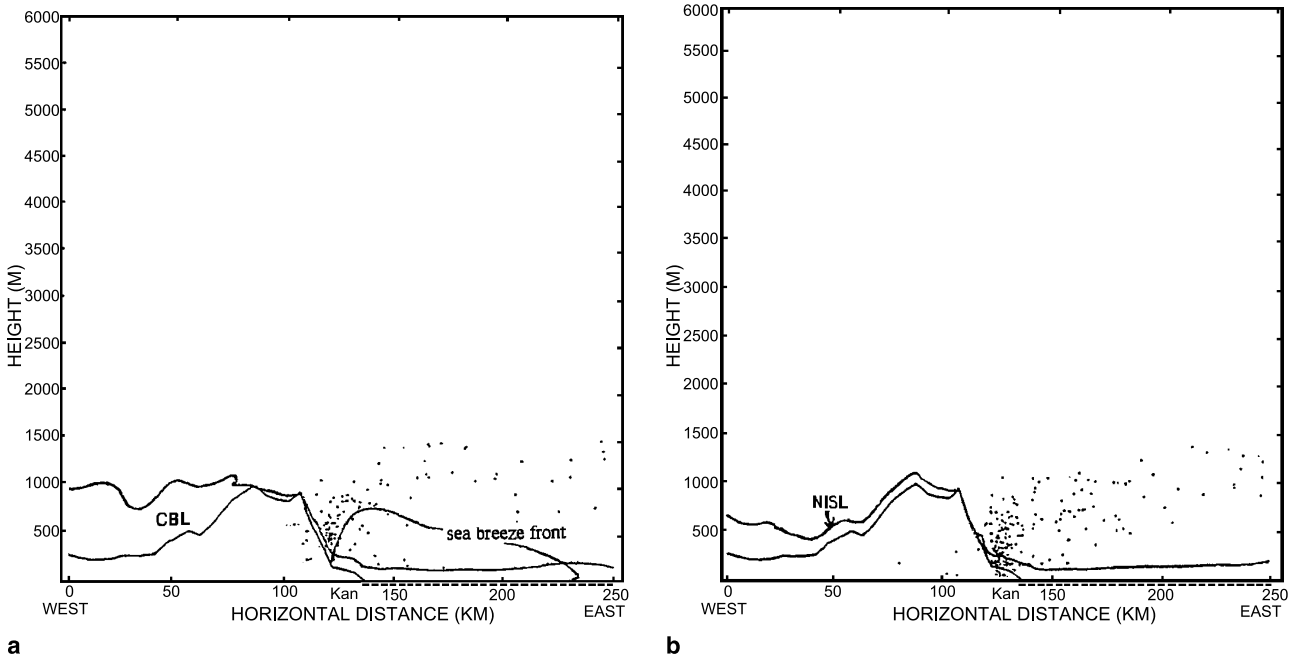


Fig. 5a. Transportation of suspended particulates in the coastal region near Kangnung city (Kan) at 1800 LST on August 14, 1995, and **(b)** as in **(a)**, except at 2100 LST. CBL denotes convective boundary layer

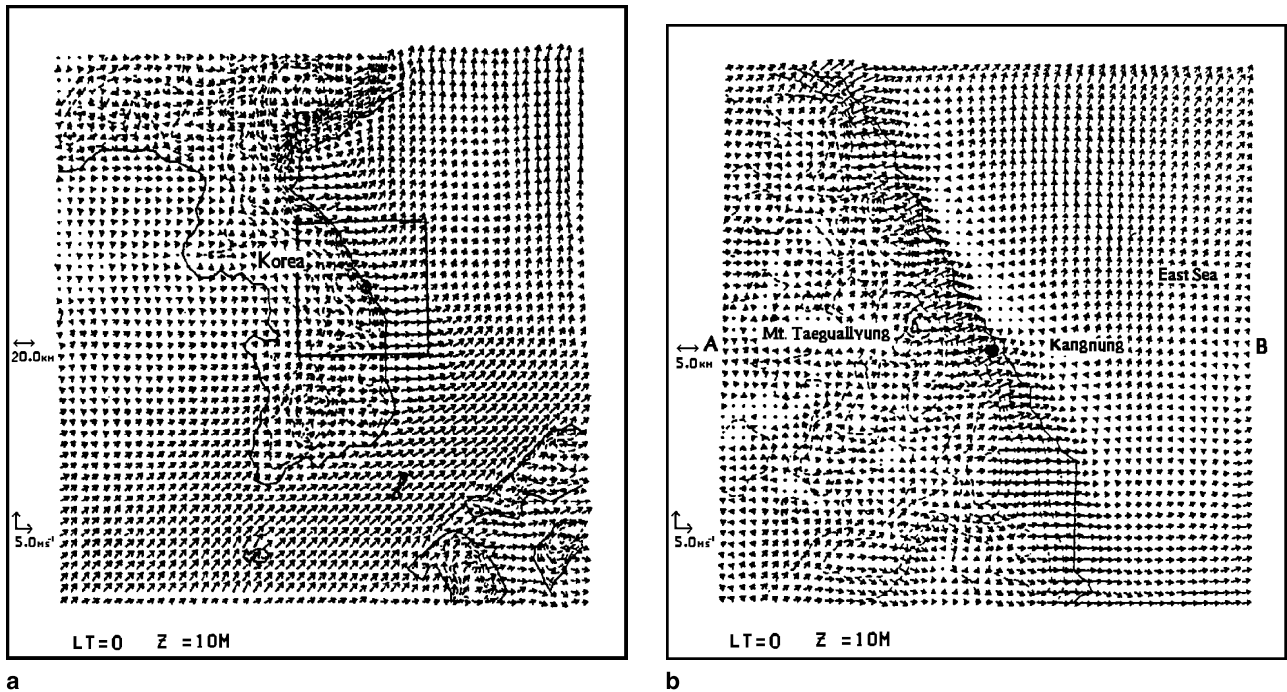
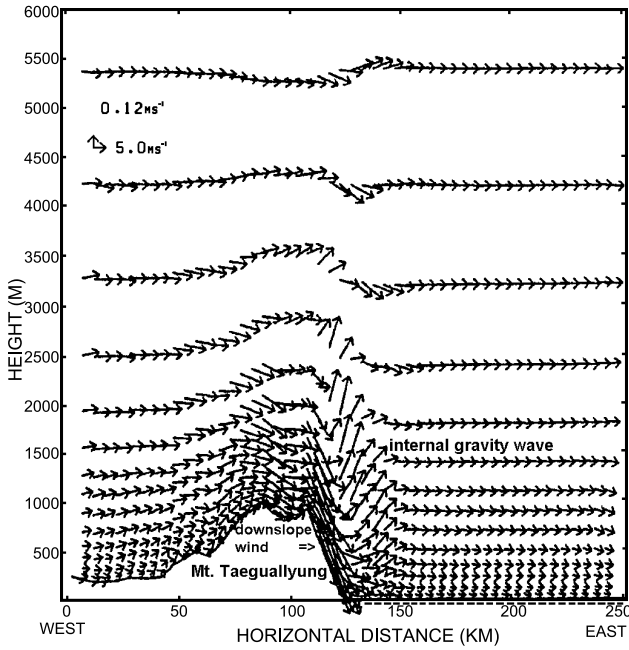


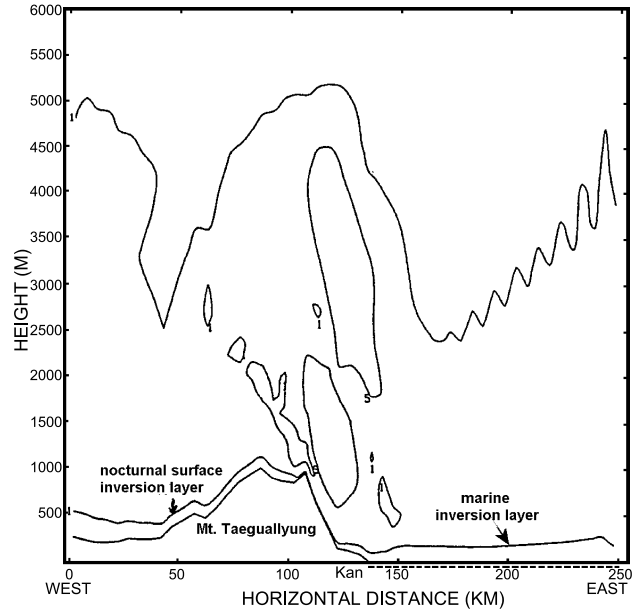
Fig. 6a. Surface wind pattern ($m s^{-1}$) in the coarse-mesh domain adjacent to the Korean peninsula at 0000 LST, August 15, 1995. The thin line (dashed) and circle (open) denote topography and Kangnung city, respectively; **b** the fine-mesh domain, as indicated by the inset in **(a)**, and showing Kangnung city

causes the wind speed to increase. Since the downslope westerly wind could penetrate into the city, particulate matter, uplifted during the

day also descends along the eastern slope of the mountains toward the centre of Kangnung city.

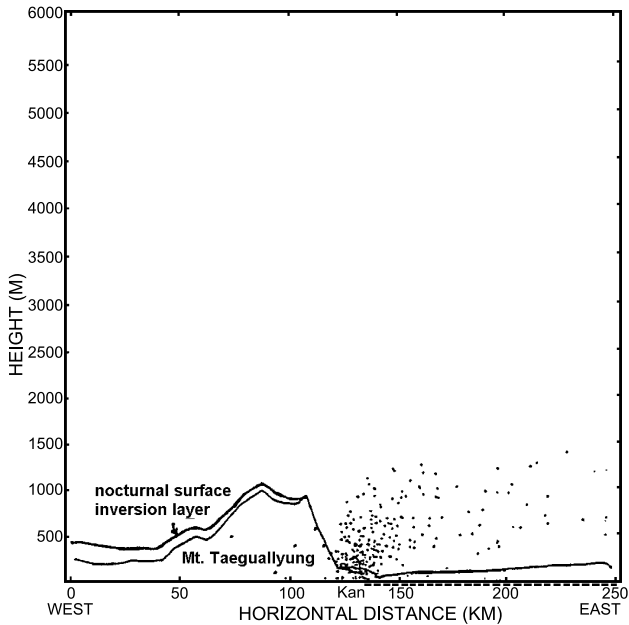


a

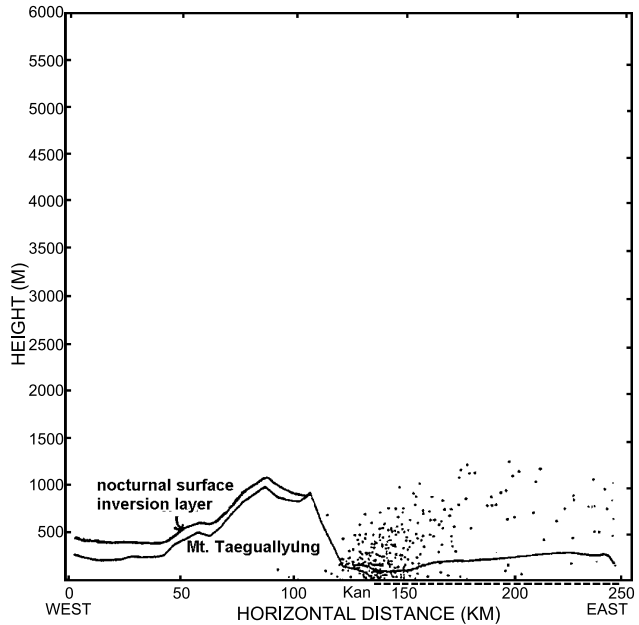


b

Fig. 7a. Vertical wind profile (m s^{-1}) at 0000 LST, August 15, 1995 through the line A–B (Mt. Taeguallung–Kangnung city–East Sea) as indicated in the fine mesh domain of Fig. 6b; **(b)** as in **(a)** except vertical diffusion coefficient for turbulent heat ($\text{m}^2 \text{s}^{-1}$)



a



b

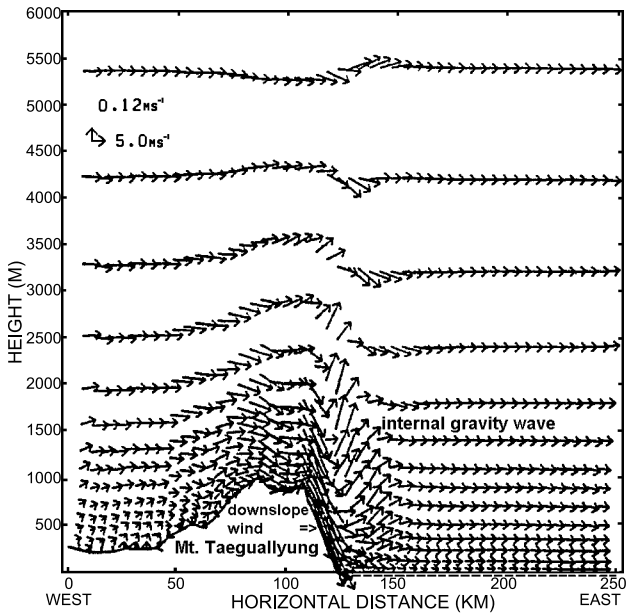
Fig. 8a. Vertical profile along A–B in Fig. 7a showing transportation of suspended particulates by strong westerly downslope wind and land breeze into Kangnung city (Kan) in the coastal region at 0000 LST, 15 August, 1995, and **(b)** as in **(a)** except at 0300 LST when maximum concentration of total suspended particulates (TSP; ug m^{-3}) occurs. Note that some particulates are forced to rise to higher tropospheric levels following the propagation of internal gravity waves and others are deposited on the sea surface

Those particulates combine with the particulates (vehicle and industrial) released from the surface of the city and generated by strong sur-

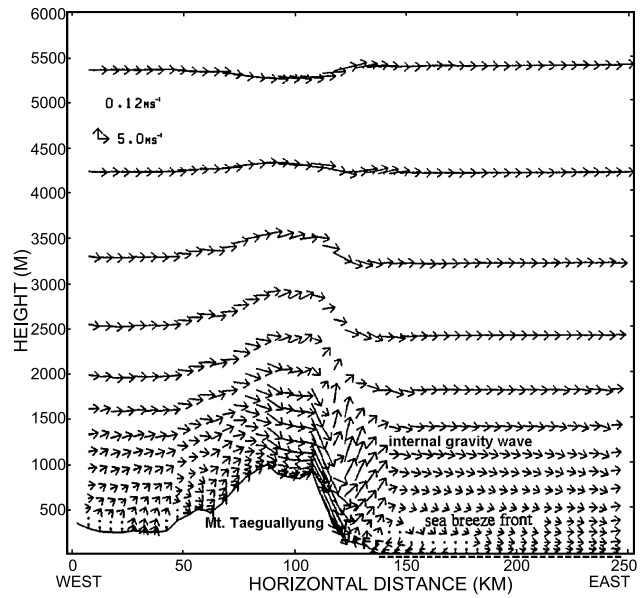
face winds, are then transported eastwards toward the coastal sea, resulting in a maximum concentration of TSP at the surface in Kangnung

city at 0000 LST. The particulates trapped inside the coastal NSIL, in general, are dispersed toward the propagation source area of internal

gravity waves. At 0300 LST and 0600 LST, the particulates move further eastward over the East Sea where some are deposited on the sea surface

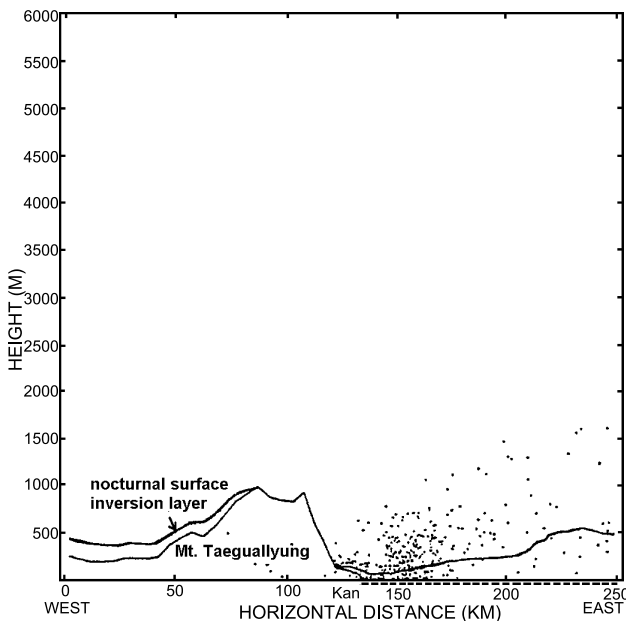


a

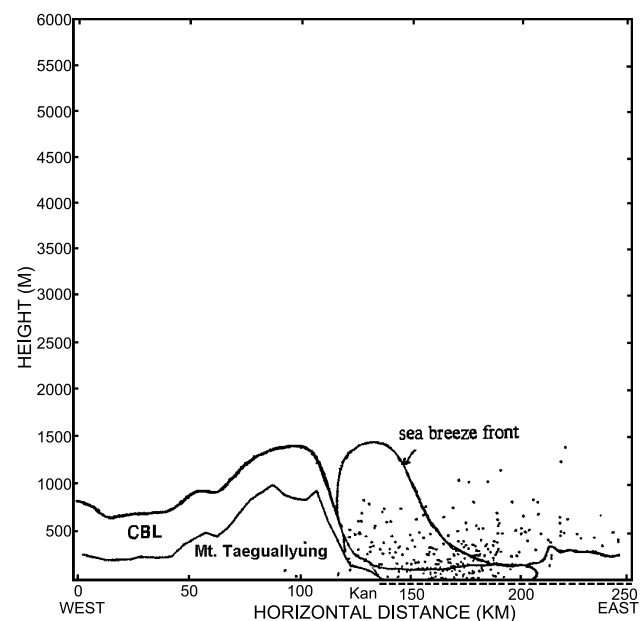


b

Fig. 9a. Vertical wind profile ($m s^{-1}$) at 0600 LST, August 15, 1995 through the line A–B (Mt. Taegualliyung–Kangnung city–East Sea) as indicated in Fig. 7a, when maximum development of internal gravity waves had occurred; **b** Three wind regimes at 0900 LST indicating the effect of westerly downdlope winds, internal gravity waves and the easterly sea breeze



a



b

Fig. 10a. Vertical profile along A–B as in Fig. 7a indicating transportation of particulates at 0600 LST, 15 August, 1995 under the combined influence of strong downdlope wind and land breeze directed into Kangnung city (Kan) in the coastal region; **(b)** as in **(a)** except at 0900 LST when some particulates have been recycled from the sea into the city by the easterly sea-breeze and combined with recycled particulates emitted from the surface of the city in the morning. These particulates, in turn, are again transported toward the top of the mountains

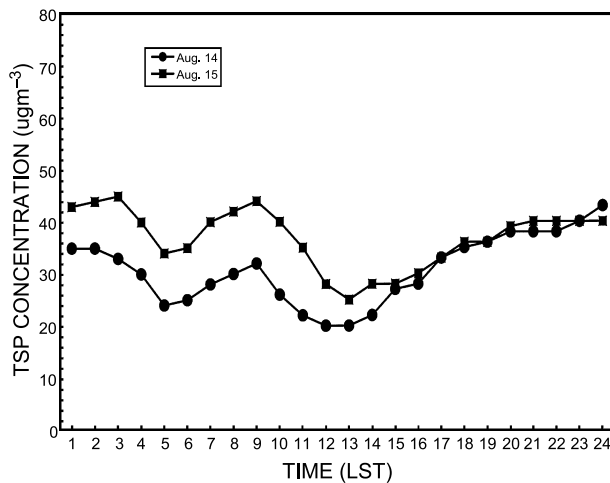


Fig. 11. Hourly concentration of total suspended particulate matter ($\mu\text{g m}^{-3}$) at the monitoring site of Kangnung city from 14 August to 15 August, 1995

itself under the influence of the strong mountain-land breeze (Figs. 9 and 10). The tendency for a low concentration of particles in the model results is well matched by the measured TSP concentration at Kangnung National University (KNU, 1995).

At 0900 LST on 15 August (following day), some of the particulates dispersed over the sea surface from the previous night return to the coastal inland basin by the easterly sea breeze. Recycled particulates combine with particulates emitted from the surface of the city in the morning and rise again from the surface toward the top of the mountains under the influence of upslope (and valley) winds. The TSP-concentration at 0900 LST is higher relative to the previous day. The tendency for a low concentration of particulates in the model result matches well the measured TSP concentration at Kangnung National University (KNU, 1995).

4. Conclusions

Modelling results over the southern Korean peninsula for the 48 h period 9 AM 13 August to 9 AM 15 August, 1995 indicate that under the influence of synoptic scale westerly winds the CBL develops to a thickness of about 1 km above the ground on the western side of the mountains, while the thickness of the TIBL is confined to less than 200 m along the eastern slope of the mountains, below an easterly sea breeze circulation. Midway along the eastern slope of the

mountains westerly winds meet the easterly sea breeze, which reaches a height of 1700 m above sea level and is finally directed to the east in a return flow toward the sea. Suspended particulates rise from the surface of the city to the top of the TIBL and are transported along the eastern slope of the mountains with the passage of the sea breeze, and reach the top of the mountains. Those particulates then disperse eastward below the height of the sea-breeze circulation and spread out widely over the coastal sea.

Total suspended particulate concentration near the surface of the city is very low. On the other hand, nocturnal radiative cooling produces a shallow nocturnal surface inversion layer (NSIL) with a thickness of about 200 m over the inland surface, but a relatively thinner thickness of less than 100 m is found near the surface at the top of the mountains.

Synoptic scale westerly winds intensify due to down motion along the eastern slope combined with the westerly land-breeze directed from the inland plain toward the sea, resulting in stronger wind speeds, internal gravity waves and a hydraulic jump effect reaching to a height of about 1 km from the surface on the western side of Kangnung city where the circulation then becomes a return flow directed eastwards. Simultaneously, wind speeds near the coast on the eastern side of the city are moderate. Since the strong downslope westerly winds penetrated the city, particulate matter that was near the top of the mountains during the day also moved down the eastern slope of the mountains, reaching the centre of Kangnung city and merged near the surface inside the NSIL. Here, a maximum ground level concentration of TSP occurred at 0300 LST on 14 August. A proportion of these particulates were forced to rise from the surface to as high as 1 km and others were transported to the coastal sea surface, as they dispersed in the coastal NSIL toward the propagation area of internal gravity waves. At 0600 LST and 0900 LST on the following day (15 August), the dispersed particulates present over the coastal sea could return to the coastal inland area under the influence of the sea breeze and the recycled particulates could combine with those emitted at the surface, resulting in a relatively higher TSP concentration. In turn, these particulates again rise toward the top of the TIBL, by the action of the sea-breeze circulation.

Acknowledgements

The authors thank the Meteorological Research Institute, Japan Meteorological Agency for the use of their Hitachi super computer and Dr. Junji Sato, in particular, for financial support. This study was in part supported by a grant-in-aid of the exchange visiting program of the Meteorological Research Institute of Japan during 1998–1999.

References

- Baird C (1995) Environmental chemistry. New York: Freeman, 484 pp
- Businger JA (1973) Turbulence transfer in the atmospheric surface layer. Proc. Workshop on Micrometeorology (Haugen DA, ed). Amer Meteor Soc 54: 67–100
- Choi H (2003) Increase of ozone concentration in an inland basin during the period of nocturnal thermal high. Water Air Soil Poll Focus 3: 31–52
- Deardoff JW (1978) Efficient prediction of ground surface temperature and moisture with inclusion of a layer of vegetation. Geophys Res 38: 659–661
- Diehl S, Smith D, Sydor M (1982) Radom walk simulation of gradient-transfer processes applied to dispersion of stack emission from coal-fired power plants. J Appl Meteor 69: 69–83
- JMRI (1995) Manual of random walk model revised by Mr. S. Takahashi, 10 pp
- Katayama A (1972) A simplified scheme for computing radiative transfer in the troposphere. Technical Report 6, Dept. of Meteor., U.C.L.A., 77 pp
- Klemp JB, Durran DR (1983) An upper condition permitting internal gravity wave radiation in numerical meso-scale models. Mon Wea Rev 111: 430–440
- Kimura F, Arakawa S (1983) A numerical experiment of the nocturnal low-level jet over the Kanto plain. J Meteor Soc Japan 61: 848–861
- Kimura F, Takahashi S (1991) The effects of land-use and anthropogenic heating on the surface temperature in the Tokyo metropolitan area: numerical experiment. Atmos Environ 25: 155–164
- Kimura F, Yoshikawa T (1988) Numerical simulation of global scale dispersion of radioactive pollutants from the accident at the Chernobyl Nuclear Power Plant. J Meteor Soc Japan 66: 489–495
- KNU (1995) Measured data of TSP by Dept. of Atmos. Environ. Sci., Kangnung National University
- Kuwagata T, Sumioka M (1991) The daytime PBL heating process over complex terrain in central Japan under fair and calm weather conditions. Part III: Daytime thermal low and nocturnal thermal high. J Meteor Soc Japan 69: 91–104
- Moller D (2001) Photooxidation capacity. Proc. Workshop on Local and Regional Contribution to Air Pollution and Local Radiative Balance in Asian Developing Countries. Guangzhou, China, 16
- Monin AS (1970) The atmospheric boundary layer. Annu Rev Fluid Mech 2: 225–250
- NFRADA (1998) Analyzed NOAA satellite picture on the sea surface temperature. National Fisheries Research and Development Agency
- Orlanski I (1976) A simple boundary condition for unbounded hyperbolic flows. J Comp Phys 21: 251–269
- Park SU, Moon JY (2001) Lagrangian particle dispersion modeling in the complex coastal terrain of Korea. J Korean Meteor Soc 37: 225–238
- PU (1995) The effects of particles and gases on acid depositions and parameterization. Technical Report of State Key Project 85-912-01-04-05, 250 pp
- Ross DG, Lewis AM, Koutsenko GD (1999) Comalco (bell bay) local airborne contaminant transport study: Airshed modeling system, development and evaluation. Proc. 5th Joint Seminar on Regional Deposition Process in the Atmosphere, Seoul, pp 43–52
- Takahashi S (1995) Manual of LAS model revised by Dr. J. Sato, 50 pp
- Xuan J (1999) Vertical fluxes of dust in northern Asia. Proc. 5th Joint Seminar on Regional Deposition Process in the Atmosphere, Seoul, pp 43–52
- Yamada T (1983) Simulation of nocturnal drainage flows by a q2-1 turbulence closure model. J Atmos Sci 40: 91–106
- Yamada T, Mellor GL (1983) A numerical simulation of the BOMEX data using a turbulence closure model coupled with ensemble cloud relations. Q J R Meteor Soc 105: 915–944
- Zhang Z, Zhou Q, Liu B (2001) Monitoring of the characters and ground-surface of dust storm area in North China remote sensing. J Remote Sens 5: 377–382

Corresponding author's address: H. Choi, Environmental Science Center, Peking University, Beijing, P.R. of China (E-mail: du8392@hanmail.net)